

Coherence transfer through homonuclear dipolar coupling in an unoriented two spin-1/2 solid-state system[☆]

D.M. Taylor^a, A. Ramamoorthy^{a,b,c,*}

^a*Biophysics Research Division, The University of Michigan, Ann Arbor, MI 48109-1055, USA*

^b*Department of Chemistry, The University of Michigan, Ann Arbor, MI 48109-1055, USA*

^c*Macromolecular Science & Engineering, The University of Michigan, Ann Arbor, MI 48109-1055, USA*

Received 2 February 2001; accepted 21 February 2001

Abstract

Dipolar coupling is a valuable NMR parameter to study the structure and dynamics of solids and partially aligned biological molecules in solution. The transfer of magnetization via the homonuclear dipolar coupling, known as dipolar coherence transfer (DCT), has been used to obtain the internuclear distances between two specific sites of interest in a biological solid. In this study, DCT for a pair of dipolar coupled spin-1/2 nuclei in a powder sample under static experimental condition is analyzed in detail by the numerical calculation of the analytical solutions for the time development of the density matrix. The density matrix evolution under the effect of the homonuclear dipolar interaction is evaluated using the product operator formalism. The effect of scalar coupling on DCT is also discussed. © 2002 Elsevier Science B.V. All rights reserved.

Keywords: Solid-state NMR; Homonuclear dipolar coupling; Scalar coupling; Coherence transfer; Powder

1. Introduction

Coherence transfer via the scalar coupling (through-bond or J coupling) is a basic concept successfully used in solution NMR experiments to determine the structure of macromolecules in solution-state [1,2]. In the solid-state, however, it is the dipolar coherence transfer (DCT), which modulates the majority of the coherence transfer between nuclei. Heteronuclear DCT is often employed in solid-state NMR experiments such as the traditional cross-polarization (CP) method to enhance the sensitivity of low- γ nuclei and/or low natural abundance nuclei [3].

In most static powder (or unoriented) samples,

overlap of broad spectral lines due to anisotropic interactions complicates the study of DCT. The r^{-3} distance dependence of the dipolar interaction, even in unoriented samples, makes the quantification of this effect attractive for use as a distance measurement tool. Previous publications have done much to clarify the strong and weak coupling effects on the spectral features of homonuclear spin-1/2 dipolar-coupled systems [4,5]. Also, two-dimensional powder pattern spectra obtained using spin-echo pulse sequence on static solids containing homonuclear dipolar-coupled spin-1/2 nuclei are reported [4,5]. Magic angle spinning (MAS) experiments [6,7] solve the problem of poor resolution caused by chemical shift anisotropy and dipolar coupling interactions. However, in doing so, the dipolar coupling interaction among the low- γ nuclei is also averaged to zero, so the distance information is lost in exchange for 'solution-like' high-resolution spectra of solid samples [6,7].

[☆] Dedicated to Professor Graham A. Webb on the occasion of his 65th birthday.

* Corresponding author. Tel.: +1-734-647-6572.

E-mail address: ramamoor@umich.edu (A. Ramamoorthy).

Several recoupling pulse sequences have been developed to selectively recover the homonuclear spin-1/2 dipolar coupling (for example ^{13}C – ^{13}C dipolar coupling) and are routinely used for the measurement of interatomic distances in polycrystalline or amorphous materials based on the homonuclear DCT process under MAS [8–11]. Therefore, a thorough analysis of DCT can aid in providing structural information for macromolecules (samples excepting isotropic liquids) such as unoriented samples of polymers, peptides or proteins embedded in the phospholipid bilayers, fibrous proteins, and also other biological solids [11,12]. In addition, such a study is also important for the design of better dipolar recovery pulse sequences as well to refine, or to explore the limitations of, existing pulse sequences [9,10].

Because of the nature of the dipolar coupling interaction between like spins, analytical solutions to study homonuclear DCT are complex even for a two-spin system. Further understanding of DCT requires a theoretical investigation of simple two-spin systems under various experimental conditions, which must be laid as groundwork for more complex arrangements of spins. Numerical simulations have been performed for large collections of spins, such as a linear arrangement of ten spins [6] but to date only equations for three spins have been published [13,14] and multi-spin arrangements await further analysis. In this paper, we will employ theoretical tools to explore various modes of homonuclear DCT in an unoriented solid-state system, consisting of two spin-1/2 homonuclei, under static experimental conditions.

The main focus of this work will be on various modes of coherence transfer as well as on the rate of coherence transfer via through space interaction, such as between directly bonded (H_{JD} , which includes both through bond and through space interactions) and approximately adjacent (H_{D}) ^{13}C atoms in polypeptides. In this work, we consider DCT without explicit effects from a separate chemical shift term and relaxation.

2. Dipolar Hamiltonian

Consider two chemically inequivalent spin-1/2 nuclei in a sample consisting of randomly oriented polycrystallites. We assume that the dipolar coupling

between the two nuclei is non-zero. Relaxation effects are not considered in the theoretical analysis presented here, so that dephasing of the magnetization results from the loss of coherence due to the random distribution of crystallites in the powder sample and also due to the evolution under the coherent homonuclear dipolar interaction.

In the rotating frame, the total Hamiltonian consists of chemical shift (H_{CS}), scalar coupling (H_{J}), and dipolar coupling (H_{D}) terms: $H_{\text{T}} = H_{\text{CS}} + H_{\text{J}} + H_{\text{D}}$. We assume that an experimental situation can be created to selectively suppress the chemical shift interaction with minimal or no effect on the remaining coupling terms in the total coupling Hamiltonian. For instance, in the simplest case of a static unoriented sample, a simple spin-echo sequence in the form of a series of π pulses can be utilized to refocus the chemical shifts and leave the scalar as well as the homonuclear dipolar couplings unaltered. However, the effects of the residual chemical shift interaction will be considered in a future work. In static solid peptides or proteins for example, H_{J} for homonuclear ^{13}C coupling is much smaller in magnitude than H_{D} and is usually neglected. For completeness, the contributions of scalar coupling as well as dipolar coupling to CT are included in our calculations of static samples whenever appropriate. Thus, we define our approximated total Hamiltonian as $H_{\text{D}} + H_{\text{J}} = H_{\text{JD}}$:

$$H_{\text{JD}} = (2D_{\text{IS}} + J)I_z S_z - (D_{\text{IS}} - J)\{I_x S_x + I_y S_y\} \quad (1)$$

where J is the scalar coupling constant and D_{IS} is the dipolar coupling frequency in the principal axis system of the dipolar interaction tensor defined as:

$$D_{\text{IS}}^{\text{PAS}} = \frac{\hbar \gamma_{\text{I}} \gamma_{\text{S}}}{4\pi r^3} [1 - 3\cos^2 \theta] \quad (2)$$

in Hertz. The angle θ defines the orientation of the principal axis system of the dipolar coupling interaction relative to the laboratory frame or the external magnetic field (B_0) of the spectrometer; r is the interatomic distance, and γ_{I} and γ_{S} are the gyromagnetic ratios of nuclei I and S, respectively. This form of the dipolar coupling is often called the ‘truncated’ or ‘secular’ dipolar coupling Hamiltonian.

In a uniaxially oriented system (samples such as a single crystal or a liquid crystal or mechanically aligned bilayers or magnetically aligned bicelles), D_{IS} is dependent only on r assuming θ is the same

Table 1

Expectation values $F_X(\theta, \phi, r, t)$ of product operators due to the evolution of the initial density matrix under the Hamiltonian H_D . The initial states are given in the leftmost column. The evolving states are to be read across the row where the corresponding coefficient F_X for $X = A$ to G can be found in Table 2. Negative signs indicate multiplication of the F_X coefficient by -1

$\downarrow \sigma(0)$	Ix	Sx	Iy	Sy	Iz	Sz	2IxSy	2IySx	2IxSz	2IzSx	2IySz	2IzSy
Ix	A	B										
Sx	B	A									- E	F
Iy			A	B					E	- F	F	- E
Sy			B	A					- F	E		
Iz					C	D	- G	G				
Sz					D	C	G	- G				
2IxSy					G	- G	C	D				
2IySx					- G	G	D	C				
2IxSz			- E	F					A	B		
2IzSx			F	- E					B	A		
2IySz	E	- F									A	B
2IzSy	- F	E									B	A

for all sites. In an unoriented system, D_{IS} gains an angular dependence through the distribution of θ . Therefore, the characteristic DCT spectrum of an unoriented system is comprised of the superposition of many frequencies resulting from the summation over the spatial distribution of D_{IS} . The time- and frequency-domain components of the response from a powder sample is determined by the random characteristic of the spatial anisotropy and produce a powder pattern spectrum popularly known as a Pake doublet powder pattern in the case of the frequency-domain, and therefore some kind of weighted approximate Fourier sum in the case of the time-domain signal [6,7].

3. Methods

Time evolution of different spin operators under the effect of homonuclear dipolar coupling between two spin-1/2 nuclei in an unoriented system was analytically calculated using the product operator formalism [1]. The respective analytical function representing the expectation value of a spin operator was summed numerically over all possible angles (θ and ϕ) that define random orientations of crystallites in the laboratory frame. The results are summarized in Tables 1 and 2. The details on the density matrix calculations were reported in our previous publication [15]. An initial state of the system, $\sigma(0)$, is specified in the first column of Table 1 and the coefficients of the product operators in the final density matrix

$F_X(\theta, \phi, r, t)$ are read across the subsequent columns in the same row. For example, the evolution of the initial density operator matrix $\sigma(0) = Ix$ under H_D (Table 1) should be read by finding Ix in the column labeled ' $\sigma(0)$ ' and then reading across to find the operators resulting from the operation of H_D and the functions in Table 2 that modulate these operators; for instance, it can be written as

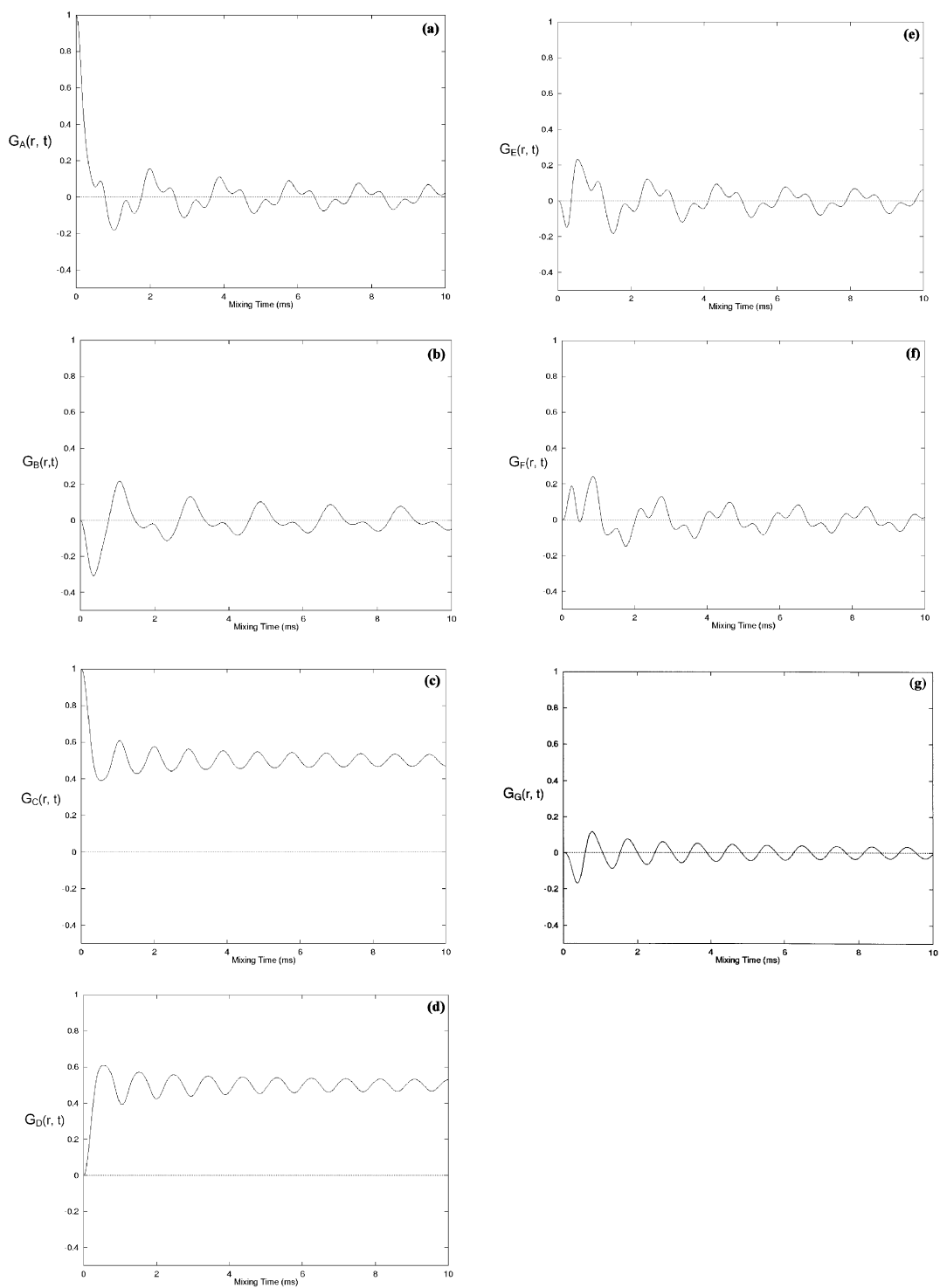
$$Ix \xrightarrow{H_D} F_A Ix + F_F IzSy - F_E IySz + F_B Sx \quad (3)$$

where the coefficients F_X can be read in Table 2. For comparison, all the simulations in this work assumed two ^{13}C nuclei at a typical glycine amino acid C_O-C_α distance of $r_{CC} = 1.53 \text{ \AA}$ corresponding to a dipolar coupling $D_{CC} = -2120.7 \text{ Hz}$. When included, isotropic scalar coupling $J = \pm 53 \text{ Hz}$. Numerical simulations of the coherence transfer functions were

Table 2

Explicit expressions for the coefficients F_X (where $X = A$ to G) as seen in Table 1 with the accompanying figures for the spatially integrated functions $G_X(r, t)$ [$\alpha = (D_{IS}/2 + J)$; $\beta = (3D_{IS}/2)$; $\gamma = (J - D_{IS})$]

X	$F_X(\theta, \phi, r, t)$	$G_X(r, t)$ in Fig.
A	$0.5(\cos(\alpha \pi t) + \cos(\beta \pi t))$	1(a)
B	$0.5(-\cos(\alpha \pi t) + \cos(\beta \pi t))$	1(b)
C	$0.5(1 + \cos(\gamma \pi t))$	1(c)
D	$0.5(1 - \cos(\gamma \pi t))$	1(d)
E	$0.5(\sin(\alpha \pi t) + \sin(\beta \pi t))$	1(e)
F	$0.5(\sin(\alpha \pi t) - \sin(\beta \pi t))$	1(f)
G	$0.5(\sin(\gamma \pi t))$	1(g)



performed using 250,000 crystallite orientations with FORTRAN programs performing a Riemann sum over the analytical coherence transfer functions weighted by the spatial distribution probability factor $P = \sin\theta d\theta$. FFT routines were available to provide frequency-domain data. Plots of DCT were created in *Gnuplot* [16] except 3-D surface plots which were created in *Mathematica* [17] with 2-D data from FORTRAN program outputs.

4. Results and discussion

To aid in the understanding of DCT in the laboratory frame, we calculated the laboratory-frame (LAB) transformation of the PAS form of H_D . This transformation makes use of unitary transformation with the Wigner rotation matrices [7] on the high-field truncated Hamiltonian H_{JD} .

The trigonometric form of D_{IS}^{LAB} can be written as follows:

$$D_{IS}^{LAB} = d_{IS} \left(\frac{3}{4} \sin^2 \theta_m \sin^2 \theta \cos(2\omega_r t + 2\phi) \right) - \frac{3}{4} \sin 2\theta_m \sin 2\theta \cos(\omega_r t + \phi) + \frac{1}{4} (3\cos^2 \theta_m - 1)(3\cos^2 \theta - 1) \quad (4)$$

The angles θ and ϕ define the random orientations of the crystallites, the angles $\omega_r t$ and θ_m are the Euler angles relating the goniometer and the laboratory frames. Fig. 3 shows that D_{IS}^{LAB} and D_{IS}^{PAS} are identical except for the tilt representing the spatial rotation by the angle θ_m ; when $\theta_m = 0$, D_{IS}^{LAB} is identical to D_{IS}^{PAS} . The term D_{IS}^{PAS} (given in Eq. (2)) is in a simpler form than Eq. (4), as its only angular dependence is on θ .

Spatial integration of each coherence transfer coefficient $F_X(\theta, \phi, r, t)$ (Table 2) yields a time-domain solution $G_X(r, t)$, which represents the expectation value of a two-spin product operator (Table 1) that

can be expressed as a spatial integral,

$$G_X(r, t) = \frac{1}{4\pi} \int_0^\pi \int_0^{2\pi} F_X(\theta, \phi, r, t) \sin\theta d\theta d\phi \quad (5)$$

where X is one of the identifiers (A, B, C, D, E, F, G), the internuclear distance is r , experimental time is t , and the spatial angles are (θ, ϕ) . It may be mentioned here that the particular analytical solution for $G_D(r, t)$ for the coefficient $F_D(\theta, \phi, r, t)$ in Table 2 resembles the classical solution for light diffracting from a half infinite plane [18] as previously shown in the literature involving an analytical solution including Fresnel integrals [19,20]. Similarly, we have shown that all of the solutions $G_X(r, t)$ derived from the numerical integration of the coefficients $F_X(\theta, \phi, r, t)$ are identical to particular combinations of similar functions involving sine and cosine Fresnel integrals [20].

When the main trigonometric argument within any $F_X(\theta, \phi, r, t)$ involves D_{IS}^{LAB} [Eq. (4)] there are no obvious analytical solutions for $G_X(r, t)$ unless $\theta_m = 0$ (when D_{IS}^{LAB} is identical to D_{IS}^{PAS}). Since D_{IS}^{LAB} is merely a spatially rotated form of D_{IS}^{PAS} (see Fig. 3), the Fresnel (and the numerically simulated) solutions $G_X(r, t)$ must be identical for both PAS and LAB forms of D_{IS} . Samples possessing partial order will require the full form of D_{IS}^{LAB} for calculation since the value of D_{IS}^{LAB} does depend on the values of individual crystallite orientations (θ, ϕ) as well as the deviation from the spherical probability distribution of $P(\theta, \phi) = \sin\theta d\theta d\phi$ used in Eq. (5). In this work, we present results for the case where $\theta_m = 0$ in D_{IS}^{LAB} , corresponding to a maximum homonuclear dipolar coupling for an oriented two spin-1/2 nuclei and sufficient for a completely unoriented sample.

Simulations of the solutions $G_X(r, t)$ for the coefficients $F_X(\theta, \phi, r, t)$ in Table 2 as a function of the evolution time under the effect of Hamiltonian H_D are given in Fig. 1(a)–(g). For example, in Fig. 1(a) the magnitude of the function $G_A(r, t)$ corresponds to the amount of normalized magnetization that remains in the source (the I nuclei) when the x magnetization of the I nuclei is selected for coherence transfer under H_D . Similarly, Fig. 1(b) represents $G_B(r, t)$,

Fig. 1. Simulations of the expectation values of the operators modulated by functions F_X (where $X = A$ to G) (given in Table 1) of an unoriented dipolar coupled two spin-1/2 system allowed to evolve freely under the effect of the homonuclear dipolar coupling Hamiltonian, H_D . Simulations assumed two ^{13}C nuclei at a typical glycine C_O-C_α distance of $r = 1.53 \text{ \AA}$ corresponding to a dipolar coupling $D_{IS} = 2120.7 \text{ Hz}$.

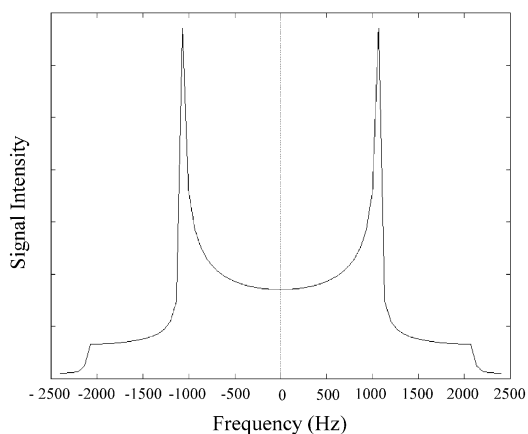


Fig. 2. The Pake doublet powder pattern spectrum obtained by the FFT of the time domain function $G_C(r, t)$ [see Fig. 1(c)] representing the longitudinal DCT mode under the effect of the homonuclear dipolar coupling Hamiltonian, H_D , of an unoriented dipolar coupled two spin-1/2 nuclei. No window function was used in FFT.

the expectation value of the S_x operator as magnetization is transferred from $I \rightarrow S$ nuclei when x magnetization of the I nuclei is selected for coherence transfer under H_D .

It can be immediately seen from Fig. 1 that longitudinal and transverse coherence transfer (for example $\sigma(0) = I_z$ or $\sigma(0) = I_x$ or I_y) modes are markedly different in character, unlike the isotropic mixing under the scalar coupling Hamiltonian in an isotropic solution. In our previous work on oriented

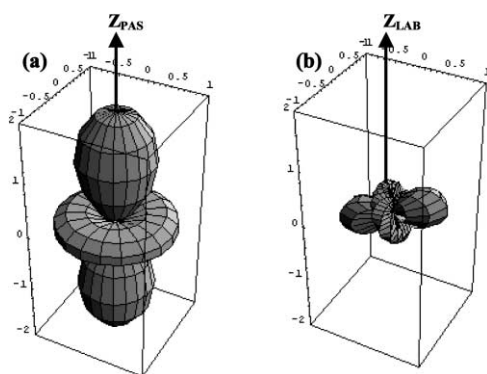


Fig. 3. The spherical plot representation of the spatial part of the homonuclear dipolar coupling Hamiltonian, H_D , of an unoriented dipolar coupled two spin-1/2 nuclei. (a) D_{IS}^{PAS} as defined in Eq. (2) in the text. (b) D_{IS}^{LAB} where $\omega, t = 0$ and $\theta_m = 57.4^\circ$ as defined in Eq. (4) in the text.

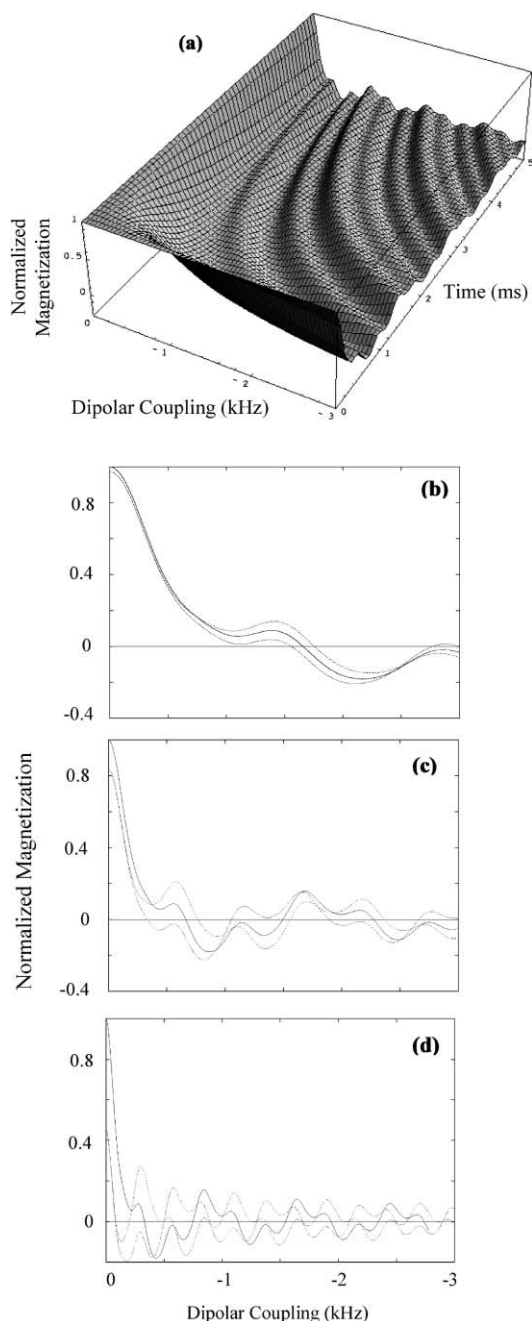
two spin-1/2 nuclei [15] we have referred to this DCT process as ‘cylindrical mixing’. Since the spin part of the dipolar Hamiltonian is identical for both oriented and unoriented systems, the evolution of the density matrix is similar in its spin part as shown in Table 1. Therefore, one would expect the different modes of DCT to be similar for oriented and unoriented samples. Indeed the longitudinal DCT leads to *in-phase* transfer of magnetization in both cases. However, a mixing time can be selected for which 100% DCT occurs in an oriented sample whereas in an unoriented sample the longitudinal DCT approaches to $\sim 50\%$ transfer only [see Fig. 1(c) and (d)]. Also, only $\sim 50\%$ magnetization remains in the source during a longitudinal DCT mode for an unoriented system while the total magnetization in the source and destination spins remains at 100%. The expectation value of the zero-quantum coherence operator ($I_x S_y - I_y S_x$), that appears when $\sigma(0) = I_z$, evolves under equation G of Table 1. G ’s maximum value is very much smaller and reaches its maxima at the time of the common intersection between the longitudinal DCT functions C and D in both oriented and unoriented samples.

Transverse modes of DCT using the x and y magnetization are identical for a given system [see Fig. 1(a) and (b)] while they are significantly different between oriented and unoriented systems. For example, in the transverse mode of DCT [corresponding to $F_A(\theta, \phi, r, t)$ and $F_B(\theta, \phi, r, t)$] a mixing time can be selected to achieve $\sim 80\%$ transfer in an oriented system as compared to $\sim 20\%$ only for an unoriented system. Further, the 20% transfer asymptotically approaches 0% for a longer mixing time due to the loss of coherence from the random distribution of various crystallites in an unoriented sample. Similarly, comparison of various modes of DCT between an oriented and an unoriented sample can be observed from the present study and previous work [15].

The unique pattern of evolution in the numerical results for all the $G_X(r, t)$ could theoretically lend themselves to detecting internuclear distances in a polycrystalline sample based on the magnitude and/or phase of dipolar coherence transfer as a function of mixing time. The Fourier transform of $G_D(r, t)$ [Fig. 1(d)] results in the typical Pake doublet shape (shown in Fig. 2). Such powder patterns have been useful to characterize the local-dynamics of a molecule in

non-isotropic phase for a known interatomic distance [6,7]. The concept of the cylindrical mixing phenomenon was recently used to understand the coherence transfer in a three spin systems related to solution NMR systems [13].

Three-dimensional plots of the efficacy of DCT as a



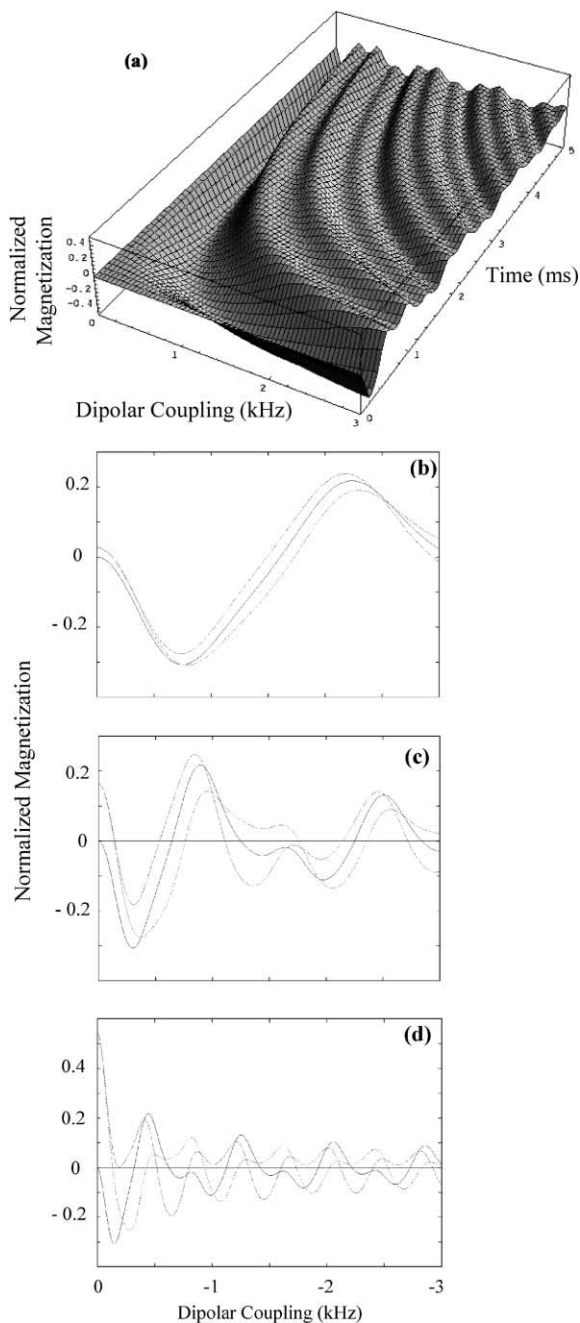
function of dipolar coupling (itself a function of r) and mixing time t are shown in Figs. 4(a), 5(a), 6(a) and 7(a) for the equivalent functions of $G_A(r, t)$, $G_B(r, t)$, $G_C(r, t)$ and $G_D(r, t)$ respectively. These plots will be useful to estimate the mixing time for optimum DCT in an experiment. Two-dimensional slices representing the dipolar coupling cross-section of the functions $G_X(r, t)$ for static mixing times 2, 5 and 10 ms are also shown in Figs. 4–7. The effect of isotropic scalar coupling ($J = \pm 53$ Hz) is shown in two-dimensional slices. The scalar coupling simply modulates the magnitude of DCT across all $G_X(r, t)$ as would be expected for an isotropic scalar coupling. Since the magnitude of D_{IS}^{LAB} has a negative value, and J can take either sign, the scalar coupling speeds or slows the efficacy of DCT depending on shared or opposed sign of D_{IS}^{LAB} . For example, in Fig. 7(b)–(d), the finely dotted line's phase appears to precede the phase of the solid line for $J = -53$ Hz, corresponding to an enhancement of the rate of DCT. On the other hand, the dashed line's phase appears to slow the phase of the solid line for $J = 53$ Hz, corresponding to a decrease in the rate of DCT.

It would be useful to study how DCT in an unoriented sample varies by internuclear distance. We begin by defining the 'maximum-DCT time' as the evolution time at which the source spin has transferred the maximum magnetization to the destination spin. We find that the first maximum-DCT in unoriented samples for a longitudinal DCT mode [Fig. 1(d)] overshoots the 50% transfer mark. This first maximum can be evaluated as shown in Fig. 8(a) for the variation of internuclear distance and the mixing time under H_D . The trace in Fig. 8(a) was generated by following the maximum-DCT time for a series of r in $G_D(r, t)$. The best-fit equation for the function shown in Fig. 8(a) was fit with *Mathematica* and is $r_{CC} = 2.67t^{1/3}$, where r_{CC} is the internuclear distance and t is the mixing

Fig. 4. (a) Three-dimensional plot of the function $G_A(r, t)$ representing the magnitude of the magnetization retained in the source spin I during DCT from I to S nuclei in an unoriented two ^{13}C homonuclear spin-1/2 (I and S nuclei) system. The initial density matrix, $\sigma(0)$, is I_x . Two-dimensional slices (b), (c), and (d) are taken from the three-dimensional plot in (a) for the evolution times 2, 5, and 10 ms respectively, shown for $J=0$ (solid lines), $J=53$ Hz (dashed lines) and $J=-53$ Hz (finely dotted lines). In (a)–(d) the variable r is represented by the dipolar coupling frequency $\nu_D = \gamma_c^2 h / (2\pi r^3)$.

time, with an R -squared fit of 1. Therefore, the maximum rate of DCT, v , in an unoriented sample can be calculated as

$$v = \frac{dr}{dt} = 0.89t^{-\frac{2}{3}}$$



and is shown in Fig. 8(b). Note the sharp drop-off in DCT rate in Fig. 8(b), where the initial velocity is well below 1 \AA/ms by 1 ms mixing time. The implication of Fig. 8 is that in powders, the summed coherence transfer behavior can be accounted for when considering rise times and maximum-DCT transfer behavior and these quantities evaluate to a simple non-trigonometric function of r and t . For example, the function for r_{CC} shows that during optimal conditions in a two-spin $1/2$ unoriented sample, maximum coherence would transfer from the source to a second site 3 \AA away in 1.42 ms. The analysis presented here can be used to design experimental studies on powder samples or partially aligned biological semi-solids. The homonuclear DCT process can be employed as a building unit in the development of multidimensional solid-state NMR methods to study the connectivity of different chemical groups or spin diffusion in non-isotropic systems. Extension of this study for various experimental conditions such as MAS and chemical shift differences between the spins that are involved in DCT will be highly useful to examine the efficacy of a pulse sequence that recovers dipolar coupling under MAS. A detailed analysis of various modes of DCT under pulse sequences that recover dipolar couplings under MAS will be published elsewhere.

5. Conclusions

A complete analysis of various modes of coherence transfer via the homonuclear dipolar coupled spin- $1/2$ nuclei in an unoriented system is presented. Theoretical DCT processes in oriented and unoriented systems are compared. The effect of scalar coupling on DCT is discussed. The results presented here provide an easy way to determine the variation of

Fig. 5. (a) Three-dimensional plot of the function $G_B(r, t)$ representing the magnitude of the magnetization retained in the source spin I during DCT from I to S nuclei in an unoriented two ^{13}C homonuclear spin- $1/2$ (I and S nuclei) system. The initial density matrix, $\sigma(0)$, is I_x . Two-dimensional slices (b), (c), and (d) are taken from the three-dimensional plot in (a) for the evolution times 2, 5, and 10 ms, respectively, shown for $J=0$ (solid lines), $J=53$ Hz (dashed lines) and $J=-53$ Hz (finely dotted lines). In (a)–(d) the variable r is represented by the dipolar coupling frequency $\nu_D = \gamma_C^2 \hbar / (2\pi r^3)$.

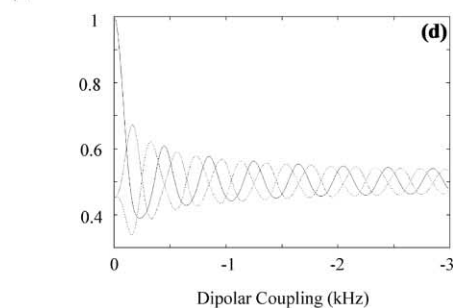
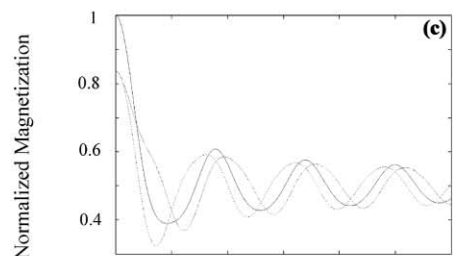
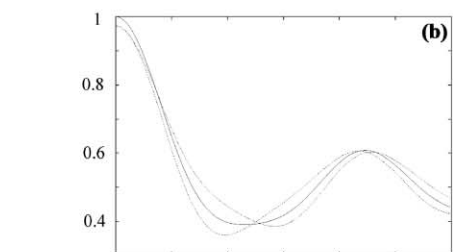
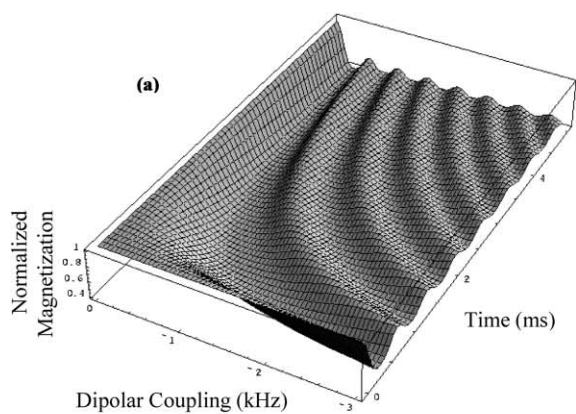


Fig. 6. (a) Three-dimensional plot of the function $G_C(r, t)$ representing the magnitude of the magnetization retained in the source spin I during DCT from I to S nuclei in an unoriented two ^{13}C homonuclear spin-1/2 (I and S nuclei) system. The initial density matrix, $\sigma(0)$, is I_z . Two-dimensional slices (b), (c), and (d) are taken from the three-dimensional plot in (a) for the evolution times 2, 5, and 10 ms, respectively, shown for $J=0$ (solid lines), $J=53$ Hz (dashed lines) and $J=-53$ Hz (finely dotted lines). In (a)–(d) the variable r is represented by the dipolar coupling frequency $\nu_D = \gamma_C^2 \hbar / (2\pi r^3)$.

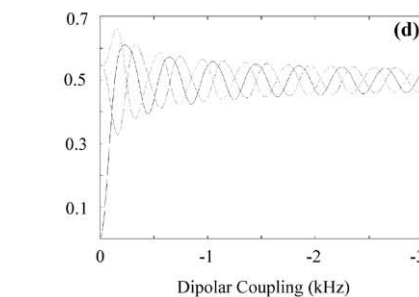
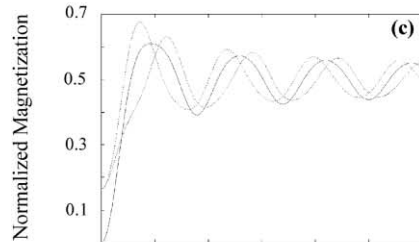
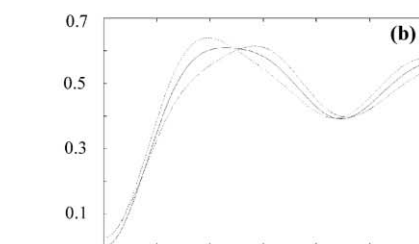
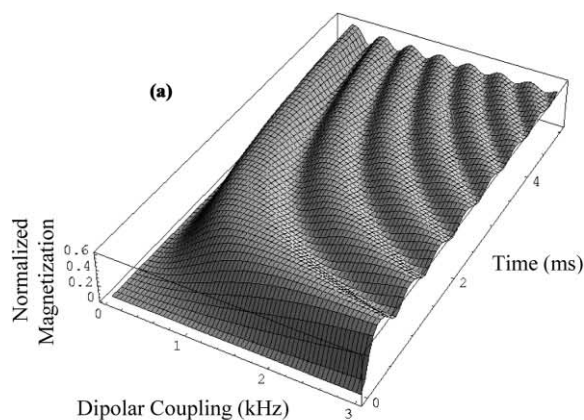


Fig. 7. (a) Three-dimensional plot of the function $G_D(r, t)$ representing the magnitude of the magnetization retained in the source spin I during DCT from I to S nuclei in an unoriented two ^{13}C homonuclear spin-1/2 (I and S nuclei) system. The initial density matrix, $\sigma(0)$, is I_z . Two-dimensional slices (b), (c), and (d) are taken from the three-dimensional plot in (a) for the evolution times 2, 5, and 10 ms, respectively, shown for $J=0$ (solid lines), $J=53$ Hz (dashed lines) and $J=-53$ Hz (finely dotted lines). In (a)–(d) the variable r is represented by the dipolar coupling frequency $\nu_D = \gamma_C^2 \hbar / (2\pi r^3)$.

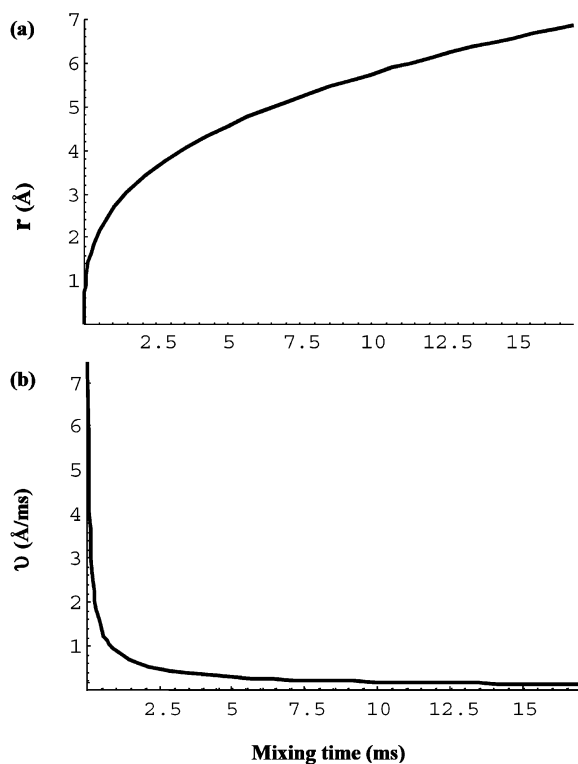


Fig. 8. (a) The trace of maximum coherence diffusion peak for the function $G_D(r, t)$ in Table 2, representing the maximum transferred longitudinal magnetization to the second spin in an unoriented two ^{13}C homonuclear spin system, for example when $\sigma(0) = I_z$. The function is fit as $r = 2.67t^{1/3}$. Scalar coupling was assumed to be zero. (b) The rate of coherence transfer, v , vs mixing time (Å/ms). $v = 0.89t^{-2/3}$ for $G_D(r, t)$.

maximum-DCT time with the internuclear distance and the mixing time.

Acknowledgements

This research was supported by the funds from NSF (CAREER Development Award to A.R.). Acknowledgment is also made to the donors of the Petroleum Research Fund, administered by the American Chemical Society, for partial support of this research.

D.M.T. would like to acknowledge the Sloan Fellowship from the University of Michigan's Center for the Education of Women.

References

- [1] R.R. Ernst, G. Bodenhausen, A. Wokaun, Principles of Nuclear Magnetic Resonance in One and Two Dimensions, Clarendon Press, Oxford, 1987.
- [2] K. Wuthrich, NMR of Proteins and Nucleic Acids, Wiley Interscience, New York, 1986.
- [3] A. Pines, M.G. Gibby, J.S. Waugh, J. Chem. Phys. 59 (1973) 569–590.
- [4] T. Nakai, C.A. McDowell, Chem. Phys. Lett. 217 (1994) 234–238.
- [5] T. Nakai, C.A. McDowell, J. Am. Chem. Soc. 116 (1994) 6373–6383.
- [6] K. Schmidt-Rohr, H.W. Spiess, Multidimensional Solid-State NMR and Polymers, Academic Press, London, 1994.
- [7] M. Mehring, Principles of High Resolution NMR in Solids, Springer-Verlag, New York, 1983.
- [8] M.H. Levitt, D.P. Raleigh, F. Cruzet, R.G. Griffin, J. Chem. Phys. 92 (1990) 6347–6364.
- [9] T. Fujiwara, A. Ramamoorthy, K. Nagayama, K. Hioka, T. Fujito, Chem. Phys. Lett. 212 (1993) 81–84.
- [10] A.E. Bennett, R.G. Griffin, S. Vega, NMR Basic Principles Prog. 12 (1994) 1–77.
- [11] S.O. Smith, K. Aschheim, M. Groesbeek, Q. Rev. Biophys. 29 (1996) 395–559.
- [12] A. Ramamoorthy, F.M. Marassi, S.J. Opella, Applications of multidimensional solid-state NMR spectroscopy to membrane proteins, in: Jardetzky, Lefevre (Eds.), Dynamics and the Problem of Recognition in Biological Macromolecules, Plenum Press, New York, 1996, pp. 237–255.
- [13] B. Luy, S. Glaser, J. Magn. Reson. 148 (2000) 169–181.
- [14] B. Luy, S. Glaser, J. Magn. Reson. 142 (2000) 280–287.
- [15] D.M. Taylor, A. Ramamoorthy, J. Magn. Reson. 141 (1999) 18–28.
- [16] T. Williams, C. Kelley, Gnuplot; a plotting program, GNU Consortium, 2000.
- [17] Wolfram Research, Inc., Mathematica, Version 5, Champaign, IL, 2000.
- [18] M. Born, E. Wolf, Principles of Optics, Cambridge University Press, Oxford, 1999 7th expanded ed.
- [19] R. Brueschweiler, Prog. NMR Spectrosc. 32 (1998) 1–19.
- [20] D. M. Taylor, Nuclear Magnetic Resonance Coherence Transfer in a Homonuclear Two Spin-1/2 Solid-State System, PhD Thesis, The University of Michigan, Ann Arbor, MI, 2001.